

Hyperreflective Foci Enhancement in a Combined Spatial-Transform Domain for SD-OCT Images

Idowu Paul Okuwobi^{1,*}, Yifei Shen^{2,3,*}, Mingchao Li¹, Wen Fan², Songtao Yuan^{2,4}, and Qiang Chen¹

¹ School of Computer Science and Engineering, Nanjing University of Science and Technology, Nanjing, China

² Department of Ophthalmology, The First Affiliated Hospital of Nanjing Medical University, Nanjing, China

³ Su Zhou Ninth People's Hospital, Suzhou, China

⁴ The Affiliated Shengze Hospital of Nanjing Medical University, Suzhou, China

Correspondence: Qiang Chen, School of Computer Science and Engineering, Nanjing University of Science and Technology, Xiao Lingwei 200#, Nanjing 210094, China. e-mail:

chen2qiang@njust.edu.cn

Songtao Yuan, Department of Ophthalmology, The First Affiliated Hospital of Nanjing Medical University, 300 Guangzhou Rd, Nanjing 210029, China. e-mail: yuansongtao@vip.sina.com

Received: June 10, 2019

Accepted: December 9, 2019

Published: February 14, 2020

Keywords: hyperreflective foci segmentation; spectral domain optical coherence tomography; image enhancement; morphological reconstruction

Citation: Okuwobi IP, Shen Y, Li M, Fan W, Yuan S, Chen Q. Hyperreflective foci enhancement in a combined spatial-transform domain for SD-OCT images. *Trans Vis Sci Tech.* 2020;9(3):19. <https://doi.org/10.1167/tvst.9.3.19>

Purpose: Spectral-domain optical coherent tomography (SD-OCT) is a useful tool for visualizing, treating, and monitoring retinal abnormality in patients with different retinal diseases. However, the assessment of SD-OCT images is thwarted by the lack of image quality necessary for ophthalmologists to analyze and quantify the diseases. This has hindered the potential role of hyperreflective foci (HRF) as a prognostic indicator of visual outcome in patients with retinal diseases. We present a new multi-vendor algorithm that is robust to noise while enhancing the HRF in SD-OCT images.

Methods: The proposed algorithm processes the SD-OCT images in two parallel processes simultaneously. The two parallel processes are combined by histogram matching. An inverse of both logarithmic and orthogonal transforms is applied to the mapped data to produce the enhanced image.

Results: We evaluated our algorithm on a dataset composed of 40 SD-OCT volumes. The proposed method obtained high values for the measure of enhancement, peak signal-to-noise ratio, structure similarity, and correlation (ρ) and a low value for mean square error of 36.72, 38.87, 0.87, 0.98, and 25.12 for Cirrus; 40.77, 41.84, 0.89, 0.98, and 22.15 for Spectralis; and 30.81, 32.10, 0.81, 0.96, and 28.55 for Topcon SD-OCT devices, respectively.

Conclusions: The proposed algorithm can be used in the medical field to assist ophthalmologists and in the preprocessing of medical images.

Translational Relevance: The proposed enhancement algorithm facilitates the visualization and detection of HRF, which is a step forward in assisting clinicians with decision making about patient treatment planning and disease monitoring.

Introduction

Hyperreflective foci (HRF) in retinal spectral-domain optical coherence tomography (SD-OCT) images were first discovered by Coscas et al.¹ They have been observed and reported in various retinal diseases, including age-related macular degeneration

(AMD), macular edema, diabetic retinopathy (DR), central serous chorioretinopathy, retinal vein occlusion, macular telangiectasia, and uveitis.² Researchers have published reports on the importance of HRF, which serve as a useful clinical feature for the treatment and diagnosis of retinal diseases. Framme et al.³ reported that HRF disappeared or were reduced drastically in patients with diffuse diabetic macular edema

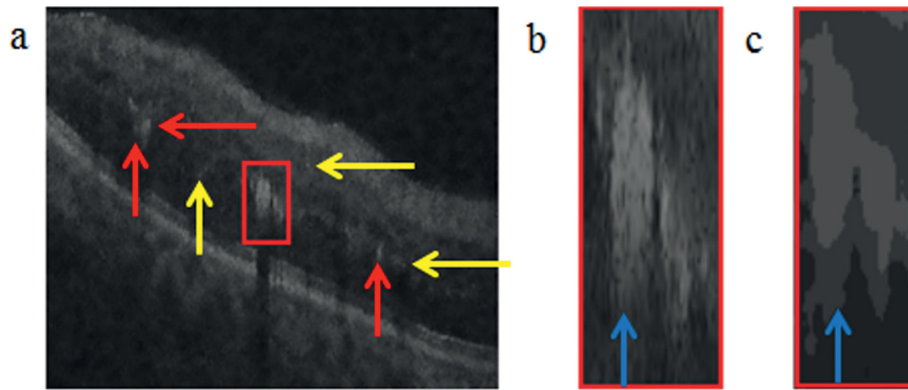


Figure 1. SD-OCT images. (a) SD-OCT image with speckle noise and HRF, (b) ROI for the image shown in (a), and (c) reconstructed ROI image of image shown in (a). The red rectangle is the ROI, the red arrows indicate the HRF, the yellow arrows indicate the speckle noise, and the blue arrows indicate the trailing and fading boundaries of the HRF. ROI, region of interest.

(DME) after anti-vascular endothelial growth factor (VEGF) treatment and in patients with focal DME. In addition, the study concluded that HRF represent a clinical marker of inflammatory response. Other studies^{4,5} have reported reductions in HRF volume after treatment, and the quantity of HRF at the control level correlated positively with the final visual outcome in exudative AMD patients after treatment with anti-VEGF. The study by Framme et al.² concluded that HRF volume regressed drastically after intravitreal ranibizumab therapy, and this decrease in volume correlated absolutely with the best corrected visual acuity (BCVA). In addition, a large initial quantity of HRF results in improved outcomes for ranibizumab therapy with respect to BCVA and edema resolution.² Furthermore, some reports have suggested that the quantity and possibly the position of HRF may be a predictive factor of the final treatment outcome for retinal diseases.

OCT is an imaging method that relies on measuring the temporal and spatial coherence of the signal reflected from the sample. As a consequence, in a highly scattering sample such as the retina, this coherence gives rise to speckle noise, which decreases the image contrast while making the highly scattering SD-OCT structure boundaries difficult to distinguish. Figure 1 shows the presence of speckle noise in a SD-OCT image. This noise imposes significant limitations on OCT diagnostic capabilities due to increased difficulty in reading and analyzing the image. Ophthalmologists depend on clearly visible and high-contrast images in disease treatment, analysis, monitoring, and diagnosis; therefore, it is necessary to reduce or eliminate the speckle noise and enhance SD-OCT images in order to utilize their interpretation for effective diagnosis and prognostic evaluation purposes.

Researchers have proposed various methods for reducing speckle noise and enhancing OCT images. Some of the spatial and transform domain techniques that have been applied are iterative deconvolution methods,^{6,7} rotating kernel transformation,⁸ wavelet analysis,⁹ and anisotropic diffusion.¹⁰ The basic limitation of these methods is serious blurring of edges, which is especially a problem when strong noise reduction is vital. To overcome these problems, better techniques have been suggested. Ying et al.¹¹ proposed a multi-exposure fusion framework for low-light image enhancement that is based on a dual-exposure fusion algorithm to provide accurate contrast and lightness enhancement. Li et al.¹² proposed a robust retinex model that additionally considers a noise map compared with the traditional retinex model to improve the performance of enhancing images accompanied by intensity noise. Researchers are also exploring various techniques that focus on suppressing speckle noise while enhancing the degraded OCT image. Chitchian et al.¹³ proposed an OCT image enhancement via shrinkage denoising using double-density, dual-tree complex wavelet transform. The authors combined two wavelet transforms to produce a locally adaptive enhancing algorithm. Anantrasirichai et al.¹⁴ proposed an adaptive-weighted bilateral filtering (AWBF) enhancement algorithm for retinal OCT images. The approach utilized multiscale despeckling based on a dual-tree complex wavelet transform for denoising and a smoothing step that adopts a novel AWBF for enhancing the OCT image.

Liu et al.¹⁵ proposed a method of enhancing OCT images based on collaborative shock filtering that involved three steps in sequence: gamma manipulation, collaborative filtering, and shock filtering. The authors denoised the noisy OCT image with a

collaborative filter following a gamma distribution and then sharpened the denoised image with a shock-type filter for edge and detail enhancement. To date, ophthalmologists have been forced to visualize HRF at uneven intensities and to view low-contrast SD-OCT images to evaluate volume changes based on the applied treatment and diagnosis. As such, an algorithm that can distinguish HRF images from their surroundings for proper visualization will be useful for ophthalmologists, as well as other researchers, in segmenting HRF. In addition, HRF are becoming an important diagnostic metric based on the rising number of reports and findings regarding their use. Several authors have reported findings on the location and quantity of HRF in relation to retinal diseases and progression.^{3,16–18} Vujosevic et al.¹⁶ reported the presence and location of hyperreflective spots in the retina in diabetic patients without clinically detectable DR or with early stages of DR (mild or moderate nonproliferative DR) without macular edema. They concluded that the number of HRF increases with the clinical progression of DR, and the HRF show an inner to outer retina migration. Uji et al.¹⁷ reported the relationship between HRF in the outer retinal layers of the external limiting membrane (ELM) at the fovea and photoreceptor integrity and visual acuity (VA). They concluded that the presence of HRF in the outer retina is closely associated with a disrupted ELM and inner segment/outer segment layer in SD-OCT images and decreased VA in DME. Bolz et al.¹⁸ analyzed HRF typically seen in DME and suggested that HRF represent extravasated lipoproteins and/or proteins, thus serving as a very early sign of subclinical barrier breakdown in DME. Aghdam et al.⁴ reported the correlation between HRF and visual and anatomical outcomes in treatment-resistant neovascular AMD. The presence and quantity of HRF have been shown to be determining factors with regard to the desired visual and anatomical outcomes after treatment of various retinal diseases.^{17,18} Several segmentation algorithms have been proposed for HRF segmentation,^{19–21} and we believe that enhancement of HRF imaging is important.

In this work, we propose a new multi-vendor algorithm that utilizes both the dynamic range and the contrast of the image to enhance HRF in SD-OCT images in a combined domain. To our knowledge, this study is the first to propose an algorithm to enhance HRF in SD-OCT images. The clinical objective of enhancing HRF images is to improve the perception and interpretability of HRF information in SD-OCT images for more effective treatment and disease monitoring, while also providing better input for medical algorithms such as automated HRF

segmentation. Those who could benefit are clinicians and computer vision programmers who perform high-level image analysis, such as target (e.g., HRF) detection or statistical analysis (e.g., quantification and measurement of HRF), on the output of the proposed algorithm.

The main contributions of the proposed algorithm include development of (1) a novel algorithm that improves HRF detection, (2) a new combined spatial-transform domain (STD) that further enhances the process, and (3) an effective mapping technique for higher to lower dynamic ranges of an image, thus making the details of HRF become distinctly clearer. Also, the original image compressibility remains unchanged, and the computational time is small.

Data Acquisition

Forty SD-OCT volumes (5120 B-scans) were acquired from 35 subjects diagnosed with various retinal diseases using Cirrus (Lifetime Vision, Grand Forks, ND, USA), Spectralis (Heidelberg Engineering, Heidelberg, Germany), and Topcon (Tokyo, Japan) SD-OCT devices. Twenty SD-OCT volumes (2560 B-scans) were acquired using the Cirrus SD-OCT device, and 10 SD-OCT volumes (1280 B-scans) each were acquired using the Spectralis and Topcon SD-OCT devices. The dataset consists of the following retinal diseases: AMD, macular edema, proliferative diabetic retinopathy, DME, central serous chorioretinopathy, neurosensory retinal detachment, and pigment epithelial detachment. Written consent forms were obtained from all patients, as well as approval of the institutional review board of the First Affiliated Hospital of Nanjing Medical University.

Methods

The proposed algorithm is shown in [Figure 2](#). The spatial transformation utilizes a transfer function (sigmoid) to control the range compression of the inputted image. Histogram equalization is applied to the output image from the sigmoid function. The resultant image from the histogram equalization is processed with two transform domain functions: orthogonal transform and then log transform. Simultaneously, the parallel process is manipulated with the two aforementioned transform domain functions. Histogram matching is applied to combine the two parallel processes together by data mapping. We applied inverse log and inverse orthogonal to the

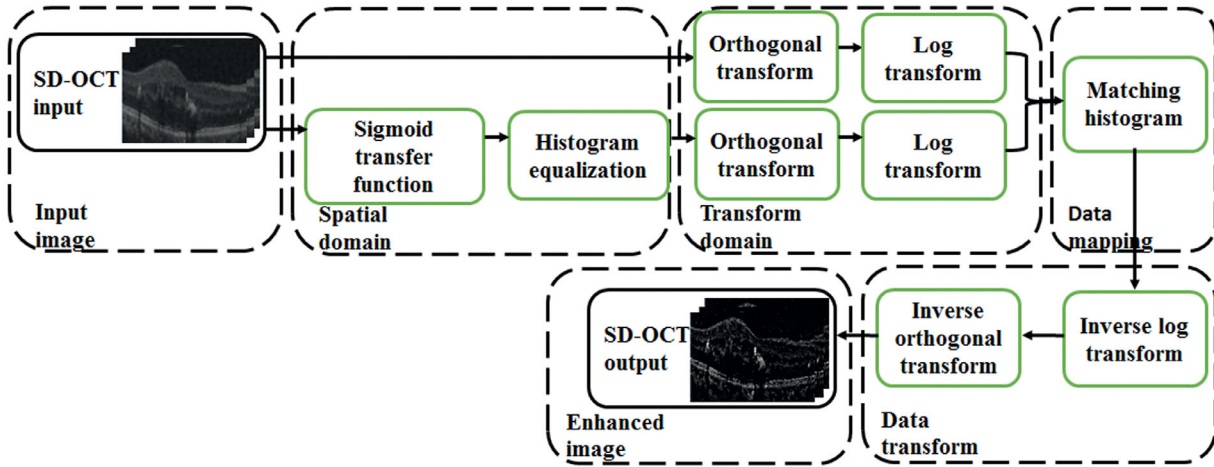


Figure 2. Flowchart for the proposed algorithm.

mapped data for data transformation to obtain the enhanced image.

Algorithm Steps

Step 1. Apply orthogonal transform to the SD-OCT input image using discrete cosine transform (DCT) by transferring the intensity information of the image into the orthogonal transform through mapping.

Step 2. Apply logarithmic transform on the magnitude values of the orthogonal transform. The resultant histogram produced by the logarithmic transform, however, was compressed and incomprehensible. To solve this problem, we created a new matrix in which the transformed image phase is preserved and is utilized by the transform coefficients for phase restoration, and we obtained the logarithm of the modulus of the transform coefficients:

$$\hat{X}(p, q) = \ln(|X(p, q)| + \lambda_s) \quad (1)$$

Here, λ_s is the shifting coefficient and is set to 1. To avoid discontinuity, the shifting coefficient factor is added to the equation. $\ln(\cdot)$ is the mapping function, and $X(p, q)$ is the image intensity.

Step 3. Apply a sigmoid transfer function to the SD-OCT input image in parallel:

$$E_{p,q} = \frac{2}{1 + e^{-2\tau_{p,q}/\rho_{stat}}} - 1 \quad (2)$$

where $\tau_{p,q}$ is the image gray level, which ranges from $0 \leq \tau_{p,q} \leq 255$ at the (p, q) location of the input image; ρ_{stat} is the statistical information of the image; and $E_{p,q}$ is the intensified pixel value. Also, ρ_{stat} is expressed as follows:

$$\rho_{stat} = (252) \left[\frac{\gamma_{p,q}}{255} \right] + k \quad (3)$$

Here, $\gamma_{p,q}$ is defined as the local mean, and k is a bias pixel value set to 3. Using a 3×3 sliding window, the local mean is obtained as follows:

$$\gamma_{p,q} = \frac{1}{N} \sum_{i=1}^N \tau_{p,q} \quad (4)$$

where N is the total number of pixels in the image. We then applied histogram equalization to the output of the sigmoid transfer function image.

Step 4. Apply an orthogonal transform using DCT to the histogram equalized image.

Step 5. Apply log transform to the orthogonal transformed magnitude values of step 4.

Step 6. Map the input image data of step 2 to match the histogram equalized image of step 5 using histogram mapping.

Step 7. Apply an inverse log transform to the matched data. The transformed image phase is restored at this step.

Step 8. Apply an inverse orthogonal transform to the exponentially processed data to produce the enhanced image (output image).

We enhanced the luminance of the image in a low-contrast SD-OCT image while preserving the global tonality of our input image by using the neighborhood-dependent intensity transformation. HRF visibility can be highly enhanced without adding irregular or unnatural details to the enhanced image in any way. We designed a new transfer function (sigmoid) to increase the dynamic range of the image and employed the hyperbolic tangent function in our dynamic range compression processes. A hyperbolic tangent function was utilized to overcome the associated loss in lightness contrast during the dynamic range compression. These functions enhanced the dark region of the input

image, in addition to retaining the light region of the image. The newly designed hyperbolic tangent function is controlled by the parameter ρ_{stat} , which makes the algorithm tunable.

In summary, we developed a new tunable hyperbolic tangent function based on image statistical characteristics, developed a SD-OCT image enhancement algorithm to preserve image details while performing a dynamic range of compression, and combined the spatial and transform domains in order to utilize the luminance and contrast features of the SD-OCT image characteristics.

Results

This section analyzes the quantitative and qualitative results obtained by our proposed method and five state-of-the-art methods.

Region of Interest

The regions of interest (ROIs), rectangular regions containing HRF, were manually annotated, as shown in Figure 1. The manually annotated ROIs were rendered to create an unbiased comparison among the five state-of-the-art methods and the proposed method.

Qualitative Analysis

B-scans from the test set using Cirrus, Spectralis, and Topcon SD-OCT devices are shown in Figure 3. We compared our proposed method with those of Ying et al.,¹¹ Li et al.,¹² Chitchian et al.,¹³ Anantrasirichai et al.,¹⁴ and Liu et al.¹⁵ The HRF ROIs are shown in Figure 4. Overall, the results show that all of the state-of-the-art methods of enhancement improved the reliability and repeatability of SD-OCT imaging as a whole; however, this overall enhancement had less of an effect on HRF regions, thus our method outperformed all five of the state-of-the-art methods.

Quantitative Analysis

Objective-Based Assessment

For the quantitative comparison, 40 SD-OCT cubes were analyzed. We used image quality metrics to evaluate the efficiency of the proposed method by computing the measure of enhancement (EME), peak signal-to-noise ratio (PSNR), structural similarity (SSIM), correlation (ρ), and mean square error (MSE) over the ROIs (Fig. 1). All of the metrics used in this work were computed as the mean over the ROIs, and we used the

measure of enhancement reported by Ying et al.⁹:

$$EME_{k_1 k_2}(\mathcal{O}) = \frac{1}{k_1 k_2} \sum_{l=1}^{k_1} \sum_{k=1}^{k_2} 20 \ln \frac{I_{max;k,l}(\mathcal{O})}{I_{min;k,l}(\mathcal{O})+c} \quad (5)$$

where an image $x(n,m)$ is divided into $k_1 k_2$ regions, (\mathcal{O}) is an orthogonal transform, $I_{max;k,l}$ and $I_{min;k,l}$ are defined as the maximum and minimum intensity values, and c is a constant.

Correlation ρ , which is used to estimate the performance of all of the algorithms based on edge preservation, is calculated as

$$\rho = \frac{\Pi(p - \mu_p, \check{p} - \mu_{\check{p}})}{\sqrt{\Pi(p - \mu_p, p - \mu_p) \cdot \Pi(\check{p} - \mu_{\check{p}}, \check{p} - \mu_{\check{p}})}} \quad (6)$$

where p is the original image and \check{p} is the intensified image in the ROIs, and Π is defined as:

$$\Pi(p_1, p_2) = \sum_{(i,j) \in ROI} p_1(i, j) \cdot p_2(i, j) \quad (7)$$

where i and j are the coordinates.

SSIM is used to estimate the structure of the original image p and the intensified image \check{p} in the ROI and is calculated as

$$SSIM(p, \check{p}) = \frac{(2\mu_p \mu_{\check{p}} + a_1)(2\sigma_{p\check{p}} + a_2)}{(\mu_p^2 + \mu_{\check{p}}^2 + a_1)(\sigma_p^2 + \sigma_{\check{p}}^2 + a_2)} \quad (8)$$

where a_1 and a_2 are constants; $a_1 = (k_1 L)$ and $a_2 = (k_2 L)$, where $k_1 = 0.01$ and $k_2 = 0.03$ are fixed constants; and L is the dynamic range of the pixel values.

Additionally, we evaluated the performance of all of the algorithms using some standard error metrics, including MSE and PSNR. Both were also calculated for pixels considered to be part of the HRF. The results of all of the algorithms using the Cirrus, Spectralis, and Topcon SD-OCT devices are shown in Table 1 and indicate that our method produced the best results. The average times required by each algorithm to enhance one B-scan using the three SD-OCT devices are shown in Table 2.

Subjective-Based Assessment

To further ascertain the potential utility of the proposed HRF enhancement algorithm, we conducted a mean opinion score analysis to compare our proposed method with the other state-of-the-art methods. To examine the differences in quality among the enhanced images obtained by all of the algorithms, three experts were asked to rate the enhanced image results based on three metrics as follows:

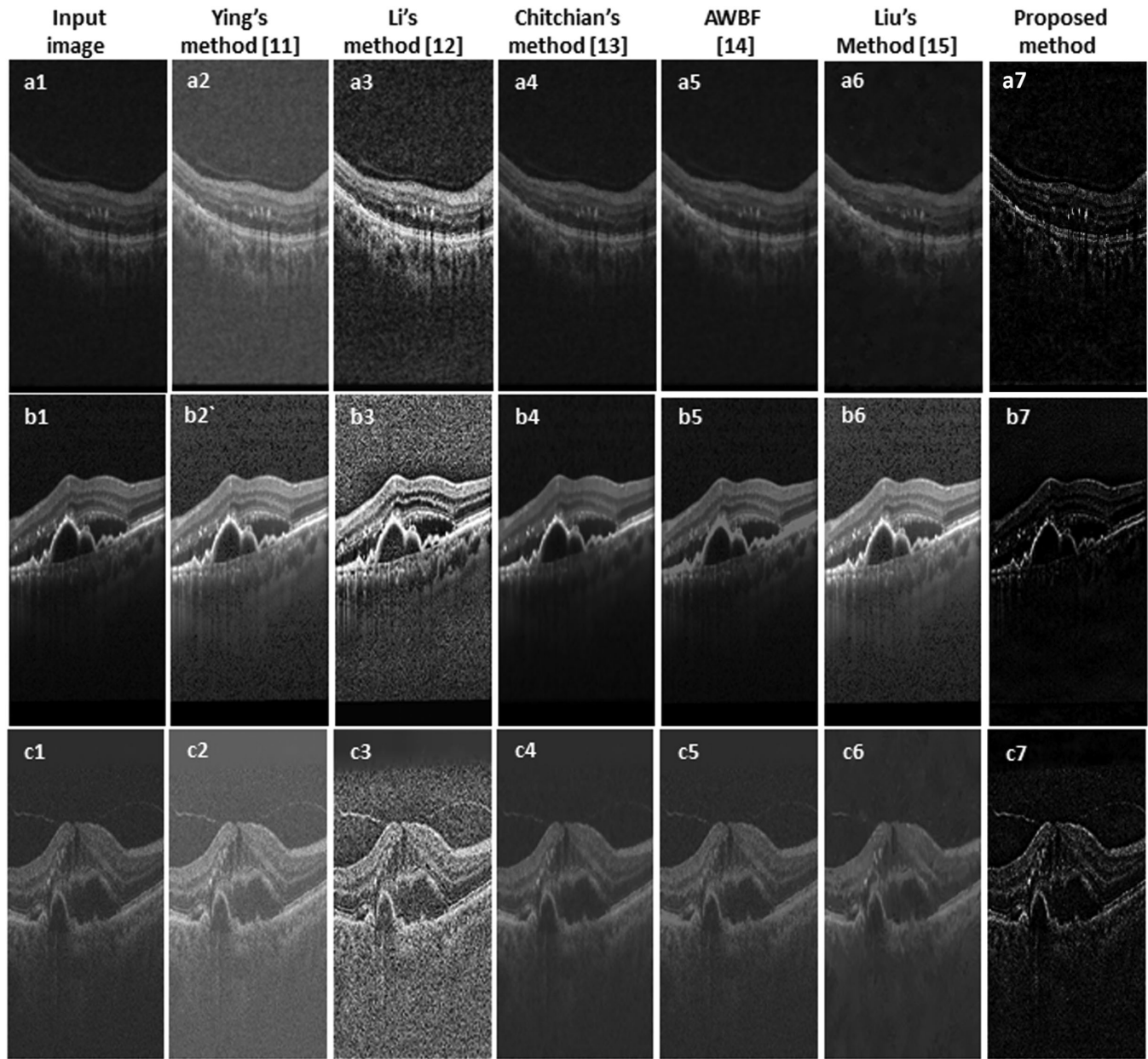


Figure 3. Enhancement results of three SD-OCT images with different algorithms using Cirrus, Spectralis, and Topcon SD-OCT devices: (a1–a7) Cirrus, (b1–b7) Spectralis, and (c1–c7) Topcon.

1. Ability to discriminate HRF (1 = most visible, 6 = least visible)
2. Accuracy at which the enhanced image shows the HRF at an indiscernible level (1 = most correct, 6 = least correct)
3. Likely usage of algorithm in medical routine (1 = most likely, 6 = least likely)

These three metrics were carefully selected in order to adequately differentiate among all of the various approaches based on visibility, accuracy, and clinical usage. Each expert was shown all of the results of the

six methods (5120 B-scan images) in an irregular order and then asked to rate each of the above three metrics. The results are shown in [Figure 5](#).

To verify differences or similarities in terms of preference among the graders for any images, we computed the inter-observer agreement as shown in [Table 3](#) using Cohen's κ score.²² Generally, the κ score is defined as a range; for example, 0.61 to 0.80 signifies substantial agreement, 0.81 to 0.99 is regarded as nearly perfect agreement, and 1 represents perfect agreement.²² The inter-observer agreement among the three experts is presented in [Table 3](#).

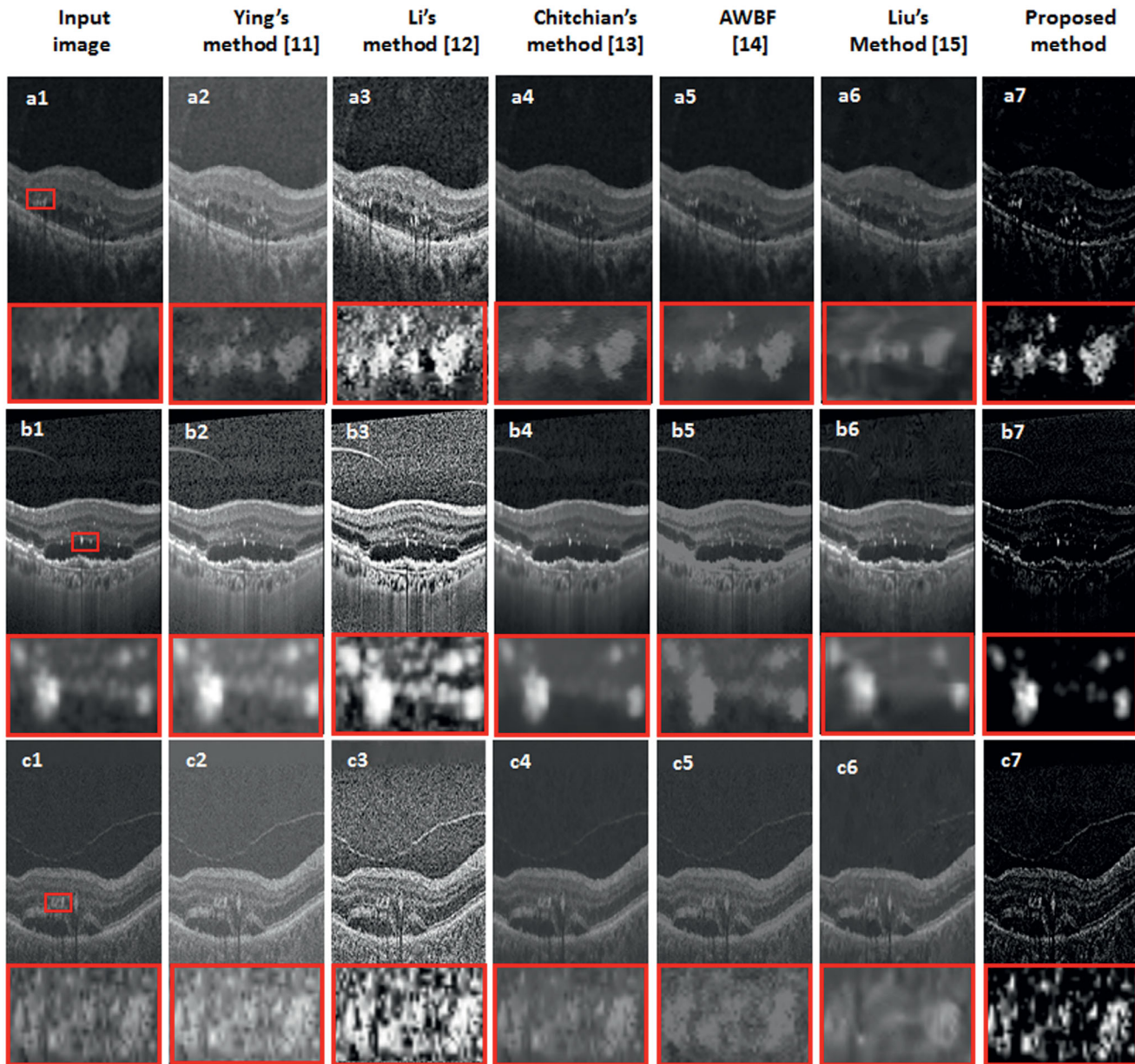


Figure 4. ROI representative output using Cirrus, Spectralis, and Topcon SD-OCT devices: (a1–a7) Cirrus, (b1–b7) Spectralis, and (c1–c7) Topcon. The red square indicates the ROI, which is enlarged 13 times for a clearer image.

It can be seen that three of the methods^{13–15} smoothed the images and provided a clearer look, whereas the methods of Ying et al.¹¹ and Li et al.¹² produced images with less HRF information for all three of the SD-OCT devices. The results based on the method of Chitchian et al.¹³ showed little improvement in the quality of the image, but the method did not destroy the needed features as compared to the methods of Ying et al.¹¹ and Li et al.¹² In contrast, our proposed method clearly enhanced HRF imaging for all three of the SD-OCT devices, even without magnifying the image. The HRF become

clearly visible when the background is suppressed. In Figure 4, the enhanced images produced by three of the methods^{13–15} show signs of smoothing, especially for the method of Liu et al.,¹⁵ where the image is blurred and the texture and boundary are faded. The boundary produced by the method of Chitchian et al.¹³ is fairly distinguishable even though the image is enlarged. In comparison, the methods of Ying et al.¹¹ and Li et al.¹² do not suppress the noise, resulting in difficulty in viewing the HRF. In Figure 4, the boundaries produced by the methods of Chitchian et al.¹³ and Anantrasirichai et al.¹⁴ are fairly comparable, whereas

Table 1. Means for EME, PSNR, SSIM, ρ , and MSE*

Evaluation Metric	Device	Mean					
		Ying et al. ¹¹	Li et al. ¹²	Chitchian et al. ¹³	Anantrasirichai et al. ¹⁴	Liu et al. ¹⁵	Proposed Method
EME	Cirrus	22.73	20.11	27.84	23.88	25.59	36.72
	Spectralis	24.87	21.05	30.98	25.19	28.74	40.77
	Topcon	14.80	11.52	20.15	17.20	19.55	30.81
PSNR	Cirrus	18.92	12.46	25.15	21.80	23.46	38.87
	Spectralis	21.70	15.62	35.10	26.83	30.33	41.84
	Topcon	12.38	10.51	19.04	15.22	18.82	32.10
SSIM	Cirrus	0.57	0.55	0.70	0.62	0.65	0.87
	Spectralis	0.59	0.56	0.72	0.63	0.61	0.89
	Topcon	0.50	0.45	0.66	0.54	0.50	0.81
ρ	Cirrus	0.51	0.53	0.92	0.91	0.90	0.98
	Spectralis	0.56	0.55	0.93	0.91	0.90	0.98
	Topcon	0.50	0.49	0.90	0.89	0.89	0.96
MSE	Cirrus	57.49	55.81	40.92	42.51	42.88	25.12
	Spectralis	55.28	55.75	39.71	40.55	40.07	22.15
	Topcon	59.58	61.07	45.35	48.83	46.41	28.55

*For 2560 Cirrus B-scans, 1280 Spectralis B-scans, and 1280 Topcon B-scans of patients with various retinal diseases.

Table 2. Time Required for All Methods to Process a Single B-Scan*

SD-OCT Device	Time (s)					
	Ying et al. ¹¹	Li et al. ¹²	Chitchian et al. ¹³	Anantrasirichai et al. ¹⁴	Liu et al. ¹⁵	Proposed Method
Cirrus	0.49	3.25	2.05	3.47	4.31	2.81
Spectralis	0.34	3.09	1.74	3.19	3.16	1.76
Topcon	0.31	3.01	1.70	3.12	3.10	1.73

*Averaged over 2560 Cirrus B-scans, 1280 Spectralis B-scans, and 1280 Topcon B-scans.

Table 3. Inter-Observer Agreement, as Measured by Cohen's κ Score, Among the Three Experts for Each of the Qualitative Metrics for the 5120 B-Scans Acquired Using Cirrus, Spectralis, and Topcon SD-OCT Devices

Metrics	1v2	1v3	2v3
Clarity	0.81	0.80	0.83
Accuracy	0.82	0.85	0.81
Preference	0.85	0.82	0.83

the method of Li et al.¹² also produced good boundary images but with unwanted regions enhanced. The method of Liu et al.¹⁵ performed better in terms of enhancement but suffered from serious blurring, as shown in Figure 4.

These results indicate that the various SD-OCT devices pose different challenges for machine learning

algorithms, and algorithm performance on each SD-OCT device varies both in efficiency and computational cost. The proposed method produces the clearest and most enhanced results, in that HRF textures, details, and boundaries were clearly visible and preserved without unnatural artifacts on the image. Our method produced enhanced images that had a high degree of accuracy for HRF structures and edges on all three SD-OCT devices. Especially, HRF boundaries, important indicators of volume, are conserved in the proposed method. In addition, the proposed method does not blur the edges of HRF even when the image is enlarged.

Features, sharpness, distinctness, and edge preservation were all lost in the state-of-the-art methods but were preserved in our proposed method. These are key properties that play an important role in accurate HRF volume measurements that are used to determine retinal pathology. The method of Liu et al.¹⁵ produced

		Clarity					Accuracy					Preference											
a1	Ying	8	90	2				a2		72	20	8				a3	65	27	5	3			
	Li	96	4						3	21	75	1					91	7	1	1			
	Chitchian	3	4	8	34	51	%			1	13	9	30	17	%		7	5	7	32	49		
	AWBF	6	6	18	70				7	44	24	20	5		21		8	10	56	5			
	Liu	4	6	9	33	48			41	26	21	9	3		8		12	10	30	40			
	Our method				2	13	85					1	14	85						3	13	84	
b1	Ying	7	20	68	5			b2	5	21	61	13			b3	4	13	68	15				
	Li	20	62	18					8	72	20					8	32	60					
	Chitchian				3	20	77		%				4	13		83	%				5	14	81
	AWBF			8	29	57	6			4	9	27	60					4	11	25	60		
	Liu				9	22	69						8	22		70					8	22	70
	Our method					7	93							6		94						4	96
c1	Ying	11	89					c2	5	66	25	4			c3	9	44	47					
	Li	95	5						8	80	12					32	68						
	Chitchian	4	6	13	30	47	%			5	23	1	25	46		%	4	6	9	30	50	1	
	AWBF	10	9	18	63				2	25	38	27	8			23	9	12	47	9			
	Liu	6	10	15	28	41				9	43	37	9	2			10	10	2	40	38		
	Our method				5	13	82						3	16		81					5	13	82
		6	5	4	3	2	1			6	5	4	3	2	1			6	5	4	3	2	1
		Ranking					Ranking					Ranking											

Figure 5. Average qualitative results for perceived clarity, accuracy, and preference (clinical usage) for 2560 B-scans using Cirrus, 1280 B-scans using Spectralis, and 1280 B-scans using Topcon SD-OCT devices ranked by three observers: (a1–a3) Cirrus, (b1–b3) Spectralis, and (c1–c3) Topcon. The values indicate the percentage of images in each rank position (1 = highest rank, 6 = lowest rank).

blurry edges and faded HRF structures upon enlargement, as shown in Figure 4. The non-smooth HRF structures coupled with the blurry edges would make it difficult to measure or evaluate the HRF. Due to the small size of HRF, there is always a need to enlarge images for visual inspection, but the methods of Liu et al.¹⁵ and Anantrasirichai et al.¹⁴ performed poorly with regard to feature, sharpness, distinctness, and edge preservation after enlargement. The method of Ying et al.¹¹ provided little information after enhancement, and the method of Li et al.¹² provided no useful information regarding the HRF before or after enlargement on all three of the SD-OCT devices. The method of Chitchian et al.¹³ performed better than the other state-of-the-art methods in terms of visual inspection and results of enlargement on all three of the SD-OCT devices. The clear edges, sharpness, visible features, and distinctness of the HRF images produced by our proposed method were found to be superior to all of the five state-of-the-art methods, advantages that are beneficial for accurate detection and measurement of HRF in OCT images.

Table 1 shows quantitative image quality values for the five state-of-the-art methods and our proposed method. The values of the five quantitative metrics—EME, PSNR, SSIM, ρ , and MSE—are averaged for the 2560 B-scans for Cirrus, 1280 B-scans for Spectralis, and 1280 B-scans for Topcon SD-OCT devices. As can be seen in Table 1, our method obtained high values for EME, PSNR, SSIM, and ρ and low values for MSE. Our method delivered the best results for all of the quantitative metrics on all three SD-OCT devices. A paired *t*-test was performed for the proposed method with statistical significance values of $P < 0.05$. All pairwise comparisons of the EME, PSNR, SSIM, ρ , and MSE results show statistical significance ($P < 0.0002$). The proposed method and the five state-of-the-art methods were implemented in MATLAB R2013a and tested on a PC with an Intel Core i5-4200U CPU at 1.60 GHz with 8 GB of RAM.

We averaged the times over the 2560 B-scans for Cirrus, 1280 B-scans for Spectralis, and 1280 B-scans for Topcon SD-OCT devices. The results obtained

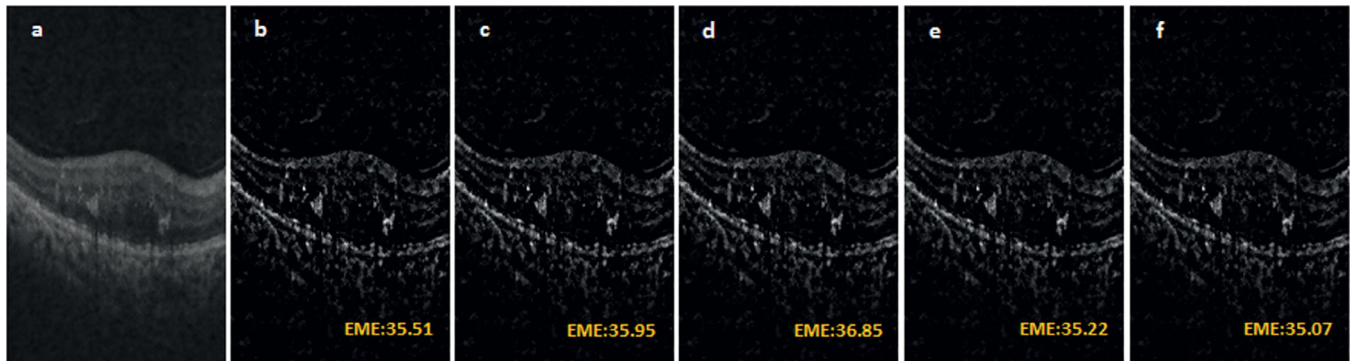


Figure 6. Varying values of κ : (a) input image; (b) $\kappa = 1$, EME = 35.51; (c) $\kappa = 2$, EME = 35.95; (d) $\kappa = 3$, EME = 35.85; (e) $\kappa = 4$, EME = 35.22; and (f) $\kappa = 5$, EME = 35.07.

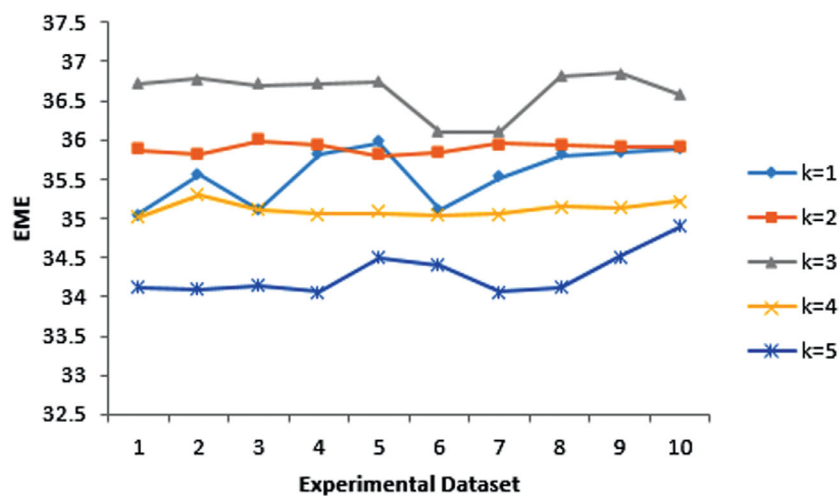


Figure 7. Effect of varying values of κ on 10 SD-OCT volumes after 5 experiments.

from all of the algorithms show that the proposed algorithm outperformed three of the state-of-the-art methods^{12,14,15} and was fairly equivalent to the method of Chitchian et al.¹³ in terms of speed of use (Table 2) on all three SD-OCT devices. Additionally, it provided outstanding results as measured by image quality metrics and visual inspection.

All three graders ranked our enhanced B-scan images highest in terms of clarity, accuracy, and clinical preference on all three SD-OCT devices. For the Cirrus SD-OCT device, our method scored no less than 84% in clarity, 93% in accuracy, and 81% in clinical preference by all three graders, indicating that the HRF images in 84% of the B-scan were the clearest, and no fewer than 13% were very clear and distinct. The same holds true for accuracy and clinical preference. Figure 5 shows that the three experts rated the images of our method notably higher than those for the five state-of-the-art methods in all three metrics on all three SD-OCT devices. The inter-observer agree-

ment reflects substantial agreement between graders 1 and 3 on clarity and nearly perfect agreement among grader 3 and the others. The high κ scores for comparisons among all of the graders indicate small variability among them.

Parameter Evaluation

The proposed algorithm is fully automated and requires no human intervention, except for the inputted image. None of the parameters was set or tuned; they were generated and processed during the enhancement process. The only parameter that was fixed for any process was the bias pixel (k), which was set to 3 as stated in Equation 3. Figure 6 shows the effect of the k value. We performed 5 experiments on 10 SD-OCT volumes to determine the optimal value for k , after which we observed that the optimal value for k is 3. It should be noted that the 10 SD-OCT volumes used to obtain the optimal value for k were not used in the test

dataset or evaluation process, but rather were used only in the fine-tuning processes for k . Figure 6 provides a representative B-scan showing that the optimal value for k is 3, with the highest EME value of 36.85. Figure 7 shows the effect of varying the values of k and confirms that $k = 3$ is optimal.

Conclusions

In conclusion, we developed a robust multi-vendor enhancement algorithm for HRF enhancement in SD-OCT images in a combined STD. The main idea of the proposed technique is to utilize the newly created STD domain to decompose the components of reflectance and illumination of the image. To achieve this, we regulate the contribution of the illumination component to compress the dynamic range of the image effectively. To compensate for the contrast, we fine-tune the reflectance component using the proposed statistical characteristic information of the image. As such, we anticipate that the algorithm will be useful for clinical diagnosis, treatment planning, and disease monitoring. But, with continued exploration and searching for better and faster techniques, we are optimistic that the efficiency and speed of the proposed algorithm might be improved in our future work.

Acknowledgments

This work was supported by the National Natural Science Foundation of China (61671242, 61701222), Key R&D Programme of Jiangsu Provincial Department of Science and Technology (BE2018131), and Suzhou Industrial Innovation Project (SS201759).

Disclosure: **I.P. Okuwobi**, None; **Y. Shen**, None; **M. Li**, None; **W. Fan**, None; **S. Yuan**, None; **Q. Chen**, None

* IPO and YS contributed equally to this article.

References

1. Coscas G, De Benedetto U, Coscas F, et al. Hyperreflective dots: a new spectral-domain optical coherence tomography entity for follow-up and prognosis in exudative age-related macular degeneration. *Ophthalmologica*. 2013;229:32–37.
2. Framme C, Wolf S, Wolf-Schnurrrbusch U, et al. Small dense particles within the neurosensory retinal layers observable by spectral domain optical coherence tomography in age-related macular degeneration. *Invest Ophthalmol Vis Sci*. 2010;51:5965–5969.
3. Framme C, Schweizer P, Imesch M, Wolf S, Wolf-Schnurrrbusch U. Behavior of SD-OCT-detected hyperreflective foci in the retina of anti-VEGF-treated patients with diabetic macular edema. *Invest Ophthalmol Vis Sci*. 2012;53:5814–5818.
4. Aghdam KA, Pielen A, Framm C, Junker B. Correlation between hyperreflective foci and clinical outcomes in neovascular age-related macular degeneration after switching to aflibercept. *Invest Ophthalmol Vis Sci*. 2015;56:6448–6455.
5. Kang JW, Chung H, Kim HC. Correlation of optical coherence tomographic hyperreflective foci with visual outcomes in different patterns of diabetic macular edema. *Retina*. 2016;36:1630–1639.
6. Rogowska J, Bryant CM, Brezinski ME. Cartilage thickness measurements from optical coherence tomography. *J Opt Soc Am A Opt Image Sci Vis*. 2003;20:357–367.
7. Schmitt JM. Restoration of optical coherence images of living tissue using the CLEAN algorithm. *J Biomed Opt*. 1998;3:66–75.
8. Rogowska J, Brezinski ME. Evaluation of rotational kernel transformation technique for enhancement of coronary optical coherence tomography images. *Proc SPIE*. 2000;doi:10.1117/12.409281.
9. Mayer MA, Borsdorf A, Wagner M, Hornegger J, Mardin CY, Tornow RP. Wavelet denoising of multiframe optical coherence tomography data. *Biomed Opt Express*. 2012;3:572–589.
10. Wang RK. Reduction of speckle noise for optical coherence tomography by the use of nonlinear anisotropic diffusion. *Proc SPIE*. 2005;doi:10.1117/12.592673.
11. Ying ZQ, Li G, Gao W. A bio-inspired multi-exposure fusion framework for low-light image enhancement. *ArXiv*. 2017;1711.00591v1:1–10.
12. Li MD, Liu JY, Yang WH, Sun XY, Guo ZM. Structure-revealing low-light image enhancement via robust retinex model. *IEEE Trans Image Process*. 2018;27:2828–2841.
13. Chitchian S, Mayer M, Boretsky AR, VanKuijk FJ, Motamedi M. Retinal optical coherence tomography image enhancement via shrinkage denoising using double-density dual-tree complex wavelet transform. *J Biomed Opt*. 2012;17:116009.
14. Anantrasirichai N, Nicholson L, Morgan JE, et al. Adaptive-weighted bilateral filtering and other

- pre-processing techniques for optical coherence tomography. *Comput Med Imaging Graph.* 2014;38:526–539.
15. Liu GH, Wang ZY, Mu GY, Li PJ. Efficient OCT image enhancement based on collaborative shock filtering. *J Healthc Eng.* 2018;2018:7329548.
 16. Vujosevic S, Bini S, Midena G, et al. Hyperreflective intraretinal spots in diabetics without and with nonproliferative diabetic retinopathy: an in vivo study using spectral domain OCT. *J Diabetes Res.* 2013;2013:1–5.
 17. Uji A, Murakami T, Nishijima K, et al. Association between hyperreflective foci in the outer retina, status of photoreceptor layer, and visual acuity in diabetic macular edema. *Am J Ophthalmol.* 2012;153:710–717.
 18. Bolz M, Schmidt-Erfurth U, Deak G, et al. Optical coherence tomographic hyperreflective foci: a morphologic sign of lipid extravasation in diabetic macular edema. *Ophthalmology.* 2009;116:914–920.
 19. Schlegl T, Bogunovic H, Klimescha S, et al. Fully automated segmentation of hyperreflective foci in optical coherence tomography images. *ArXiv.* 2018;1805.03278v1:1–12.
 20. Okuwobi IP, Fan W, Yu CC, et al. Automated segmentation of hyperreflective foci in spectral domain optical coherence tomography with diabetic retinopathy. *J Med Imaging (Bellingham).* 2018;5:014002.
 21. Okuwobi IP, Ji Z, Fan W, et al. Automated quantification of hyperreflective foci in SD-OCT with diabetic retinopathy. *IEEE J Biomed Health Inform.* 2019;doi:[10.1109/JBHI.2019.2929842](https://doi.org/10.1109/JBHI.2019.2929842) [Epub ahead of print].
 22. McHugh ML. Interrater reliability: the kappa statistic. *Biochem Med (Zagreb).* 2012;22:276–282.